Dependence upon mass number and neutron excess of the real part of the proton optical potential for mass numbers $44 \leq A \leq 72$

M. Jaminon, J.-P. Jeukenne, and C. Mahaux
Université de Liège, Institut de Physique B5, B-4000 Liège 1, Belgium
(Received 13 February 1986)

We perform detailed theoretical and empirical investigations of the real part of the optical-model potential for protons with energy $9 \leq E \leq 12$ MeV and targets with mass number $44 \leq A \leq 72$, in order to clarify earlier claims that in this domain the potential depth presents a peculiar dependence upon the target mass number A, asymmetry parameter α, and isospin T. We compile several radial moments of the empirical potentials and compare them with those predicted by a nuclear matter approach based on Reid's hard core nucleon-nucleon interaction. We find that this theoretical model is in good agreement with the empirical properties. In particular, the theoretical potential depends upon T for fixed α. This is due to the dependence upon A of its isoscalar component. The calculated potential is found to have approximately a Woods-Saxon shape with a fixed geometry, except in the surface tail where the theoretical model is, in any case, unreliable.

I. INTRODUCTION

Perey *et al.*[1,2] have analyzed the elastic scattering of 11 MeV protons by isotopes in the mass range $48 \leq A \leq 72$. They adopted a Woods-Saxon shape for the real part $V(r)$ of the optical potential,

$$V(r)=\frac{-U}{1+\exp[(r-R)/a]}\ , \tag{1.1}$$

$$R=r_0 A^{1/3}\ . \tag{1.2}$$

They assumed that the geometry is "fixed," i.e., that r_0 and a are independent of A, and found that the potential depth U is then a linear function of A. This will be exhibited in Fig. 16 below. The empirical values found by Perey *et al.*[2] are

$$r_0=1.285 \text{ fm},\quad a=0.65 \text{ fm}\ , \tag{1.3}$$

$$U \approx 40.5+0.13A \text{ MeV}\ . \tag{1.4}$$

Since we shall only deal with the real part of the optical-model potential, we henceforth refer to $V(r)$ as the optical potential. Equation (1.4) implies that the empirical depths approximately fall on a family of straight lines when plotted versus the asymmetry parameter,

$$\alpha=(N-Z)/A\ . \tag{1.5}$$

Each of these straight lines is associated with a specific value of the isospin,

$$T=(N-Z)/2\ . \tag{1.6}$$

These straight lines correspond to a linear decrease of U with increasing α, for fixed T. This will be illustrated by Fig. 17 below. As emphasized by Perey *et al.*,[1,2] this finding is at variance with the "expected" isospin dependence of the optical potential, according to which U would increase linearly with increasing α, and would furthermore be independent of T.

The dependence of U upon T for fixed α has recently been referred to as a "fine structure" by Hodgson,[3] who had previously[4] emphasized that the fine structure invalidates the usual method of determining the symmetry component of the real part of the optical potential, and that its existence hinges upon the assumption that the potential shape has a "fixed geometry." A theoretical guide is therefore needed for determining the radial shape of the optical potential. Interest in this problem has recently been renewed by the observation[3] that theoretical investigations of the radial shape of the optical potential make one expect that it does not have a "fixed geometry." These investigations are based on a nuclear matter approach to the optical potential.[5]

The main purpose of the present paper is threefold. Firstly, we perform (Sec. II) an extended compilation of the radial moments of the empirical proton optical potentials in the domain $44 \leq A \leq 72$. Secondly, we investigate (Sec. III) to what extent the main features of these moments are accounted for by the nuclear matter approach. Thirdly, we show (Sec. IV) that the calculated potentials approximately have a Woods-Saxon shape with a fixed geometry, which, however, significantly differs from that of Perey *et al.*[2]

II. MAIN PROPERTIES OF THE EMPIRICAL OPTICAL POTENTIALS

Since the original measurements and analyses of Refs. 1 and 2, many other measurements and optical-model fits have been performed in the same range of mass numbers, for protons with energy close to 11 MeV. Here we use the compilation of Ref. 6, from which we only retain the optical potentials which yield "very good," "good," or "satisfactory" fits to the experimental data, for protons with energy $9 \leq E \leq 12$ MeV and targets with mass number $44 \leq A \leq 72$. Our compilation involves 83 optical potentials, among which 18 are the potentials of the original

analysis by Perey *et al.*[2] So as not to blur the figures too much, we plot the average of the empirical values associated with a given isotope, and represent the amount of scatter of these empirical values by a vertical "error bar" whose size is equal to 2 times the standard deviation from the mean. In order to facilitate the comparison between these averages and the values originally obtained in Refs. 1 and 2, the latter are also shown and represented by crosses.

A. Volume integral per nucleon

The global attractiveness of the optical potential is usually characterized by its volume integral per nucleon,

$$[r^2]=J/A=-\frac{4\pi}{A}\int V(r)r^2dr\ , \tag{2.1}$$

which is believed to be a quantity that the elastic scattering data can determine rather accurately.[7,8]

The empirical values of J/A are plotted versus A in Fig. 1. In the domain $44\leq A\leq 72$, they are approximately independent of A (E in MeV):

$$J(E=11)/A\approx 497\pm 10\ \text{MeV fm}^3\ . \tag{2.2a}$$

In order to investigate whether this property also holds in another energy domain for the range of values of A considered here, we compiled the empirical values of J/A for protons with energy $29.5\leq E\leq 30.5$ MeV. The results are shown in Fig. 2. The data are much more sparse than at $E\approx 11$ MeV. They are compatible with the constant value

$$J(E=30)/A=408\pm 10\ \text{MeV fm}^3\ . \tag{2.2b}$$

The observation that J/A is approximately independent of A in the case of the proton optical potential is in keeping with previous results concerning the domains $12\leq A\leq 208$, $E\approx 15$ MeV (Ref. 10) and $45\leq A\leq 80$, $E\approx 5$ MeV (Ref. 11); $A=28,40,64,66,68,208$ and $E<80$ MeV (Ref. 12)

The approximate independence of J/A upon A is expected from the simplest version of the folding model,[7] according to which the optical potential is given by

$$V(r;E)=\int \rho(r')v(|\mathbf{r}-\mathbf{r}'|)d^3r'\ , \tag{2.3}$$

where $\rho(r)$ denotes the nucleon density distribution, while $v(|\mathbf{r}-\mathbf{r}'|)$ is an effective nucleon-nucleon interaction, averaged over spin and isospin. Equation (2.3) predicts that the volume integral per nucleon is equal to the volume integral of the effective interaction,[7]

$$J/A=-\int v(r)d^3r=\mathscr{V}\ , \tag{2.4}$$

and is thus independent of A.

In an improved version of the folding model[13] one takes into account the fact that the strength of the effective interaction v_{pp} between two protons is weaker than that of the effective interaction v_{pn} between a proton and a neutron, and one writes

$$V(r;E)=\int \rho_p(r')v_{pp}(|\mathbf{r}-\mathbf{r}'|)d^3r' + \int \rho_n(r')v_{pn}(|\mathbf{r}-\mathbf{r}'|)d^3r'\ , \tag{2.5}$$

where $\rho_p(r)$ and $\rho_n(r)$ denote, respectively, the proton and neutron distributions. Equation (2.5) yields

$$J=Z\mathscr{V}_{pp}+N\mathscr{V}_{pn}\ , \tag{2.6}$$

where, e.g.,

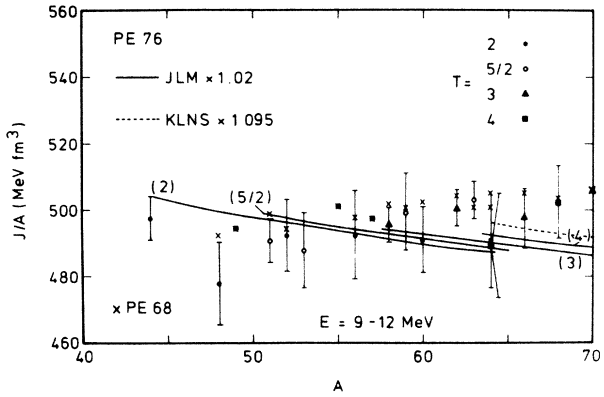

FIG. 1. Dependence upon the target mass number A of the volume integral per nucleon of the optical potential for protons with energy $9\leq E\leq 12$ MeV. The average of the empirical values associated with a given target is represented by a solid dot ($T=2$), an open circle ($T=\frac{5}{2}$), a triangle ($T=3$), or a square ($T=4$). The size of the vertical bars is equal to 2 times the standard deviation from the average. The crosses show the empirical values originally deduced by Perey *et al.* (Refs. 1 and 2). The solid curves represent theoretical values calculated from the nuclear matter approach of Ref. 5, as described in Sec. III B, multiplied by a renormalization factor $\lambda_{JLM}=1.02$. For $T=2$, these values practically coincide with those calculated from the parametrization of Ref. 9, provided the latter are multiplied by $\lambda_{KLNS}=1.095$. With this renormalization, the values of J/A calculated from the two approaches slightly differ for other values of T, as illustrated by the short dashes in the case $T=4$.

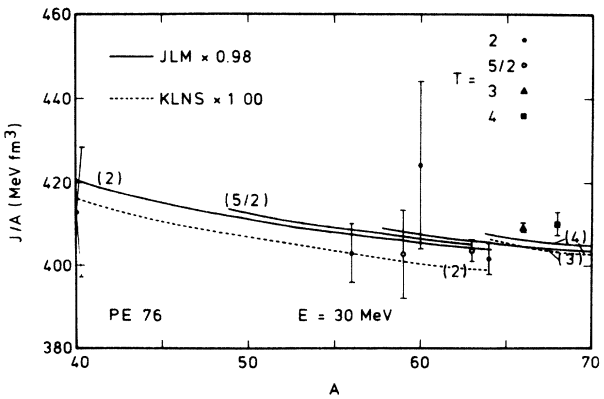

FIG. 2. Same as Fig. 1, for protons with energy $29.5<E<30.5$ MeV. A renormalization coefficient $\lambda_{JLM}=0.98$ is introduced in the case of Ref. 5. The results associated with Ref. 9 are shown only for $T=2$ and 4.

$$\mathcal{V}_{pp} = -\int v_{pp}(r) d^3r \ . \tag{2.7}$$

Introducing

$$J_0/A = \tfrac{1}{2}(\mathcal{V}_{pp} + \mathcal{V}_{pn}), \quad J_1/A = \tfrac{1}{2}(\mathcal{V}_{pn} - \mathcal{V}_{pp}) \ , \tag{2.8}$$

Eq. (2.6) yields

$$J/A = (J_0/A) + \alpha(J_1/A) \ . \tag{2.9}$$

This suggests that J/A should increase linearly with α. However, this expectation is not confirmed by Fig. 3, in which the empirical values of J/A exhibit no systematic evidence for a dependence upon α.

B. Asymmetry parameter, mass number, and isospin

In most works it is considered that a specific dependence upon A implies a specific dependence upon α, because on the average A and α are related *along* the stability band, see, e.g., Ref. 10. We emphasize that this type of relation can only indicate a global trend. It is not accurate in the small domain of mass numbers considered here, i.e., *within* the stability band. This is exhibited in Fig. 4, where A is plotted versus α. Each dashed curve is associated with a given value of T and is a portion of an hyperbola, since

$$\alpha A = 2T \ . \tag{2.10}$$

Occasionally we shall use the following linear approximation:

$$\bar{\alpha}(A) = 0.0029(A - 26.3) \ . \tag{2.11}$$

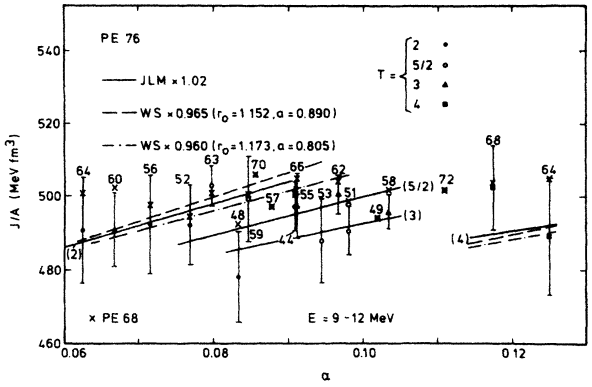

FIG. 3. Dependence upon the asymmetry parameter α of the volume integral per nucleon of the optical potential for protons with energy $9 \leq E \leq 12$ MeV and targets with mass number $44 \leq A \leq 72$. The value of A is attached to each vertical bar. The solid lines represent theoretical values calculated from Ref. 5 with the same renormalization coefficient $\lambda_{JLM} = 1.02$ as in Fig. 1. The long-dashed and dashed-dotted lines correspond to theoretical values obtained from a Woods-Saxon (WS) potential adjusted to the theoretical potential calculated with $t = 1.5$ and 1.2 fm, respectively. In the former case, the renormalization coefficient is $\lambda_{WS} = 0.965$, while in the latter case, $\lambda_{WS} = 0.960$.

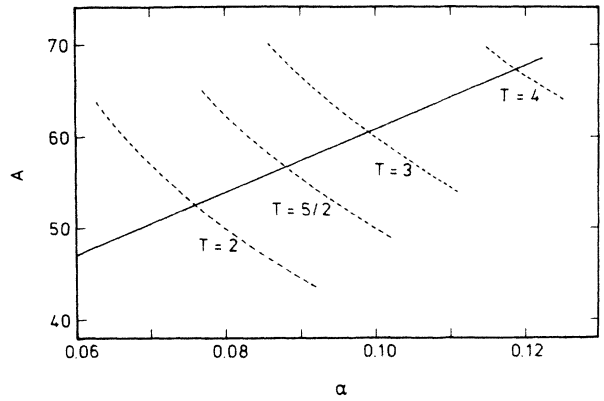

FIG. 4. Each dashed curve represents the dependence of the mass number A upon the asymmetry parameter α for a given value of the isospin T. The solid line corresponds to the average increase of A with α around the stability line, as parametrized by Eq. (2.11).

This relation is represented by the solid line in Fig. 4. It is meaningful only in the range of mass numbers considered here and describes an *average* trend, as indicated by the bar over α.

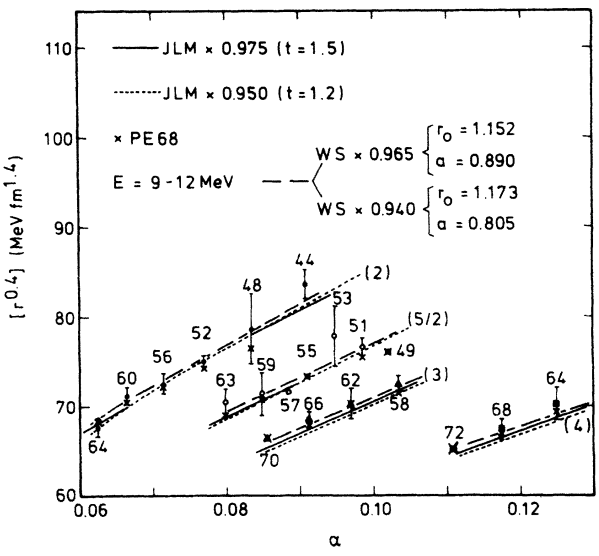

FIG. 5. Dependence upon the asymmetry parameter α of the quantity $[r^{0.4}]$ defined by Eq. (2.12). The notation is the same as in Figs. 1 and 3. The short-dashed lines represent results calculated from the nuclear matter approach of Ref. 5, after renormalization by a factor $\lambda_{JLM} = 0.95$, for a range parameter $t = 1.2$ fm; the long-dashed lines are associated with the corresponding Woods-Saxon fit (4.3), after renormalization by a factor $\lambda_{WS} = 0.940$. The results calculated in the case $t = 1.5$ fm are very close to those obtained in the case $t = 1.2$ fm, if one adopts the renormalization factor $\lambda_{JLM} = 0.975$ for the nuclear matter calculation (solid lines) and $\lambda_{WS} = 0.965$ for its Woods-Saxon fit [Eq. (4.4), long-dashed lines].

C. Weighting factor $r^{0.4}$

It has recently been pointed out that the quantity

$$[r^{0.4}]=-\frac{4\pi}{A}\int V(r)r^{0.4}dr \tag{2.12}$$

is more accurately determined than J/A by the experimental data, in the case of ^{40}Ca and ^{208}Pb.[14,15]

The dependence of $[r^{0.4}]$ upon the asymmetry parameter α is shown in Fig. 5, for the same empirical potentials as those used in Figs. 1 and 3. The comparison between Figs. 3 and 5 shows that in the present compilation the empirical values of $[r^{0.4}]$ are at least as well determined as those of J/A. This feature is not trivial in view of the difference between the integrands which appear in the definitions (2.1) and (2.12) of these two quantities; this difference is exhibited in Fig. 6.

Figure 5 displays a fine structure for $[r^{0.4}]$, in the sense that this quantity depends upon both α and T. However, Fig. 7 shows that this fine structure merely reflects the property that $[r^{0.4}]$ depends smoothly upon the target mass number A. Indeed, Eq. (2.10) implies that any quantity which is a function of A shows a "fine structure" when plotted versus α (also see Fig. 4). The stronger the dependence upon A, the more pronounced the fine structure. While the simple folding model (2.3) suggests that the volume integral J is proportional to A, no similar property is expected for the integral on the right-hand side of Eq. (2.12). Therefore, the dependence upon A, and thus upon α, of the quantity $[r^{0.4}]$ is largely influenced by the factor A^{-1} which appears in its definition (2.12).

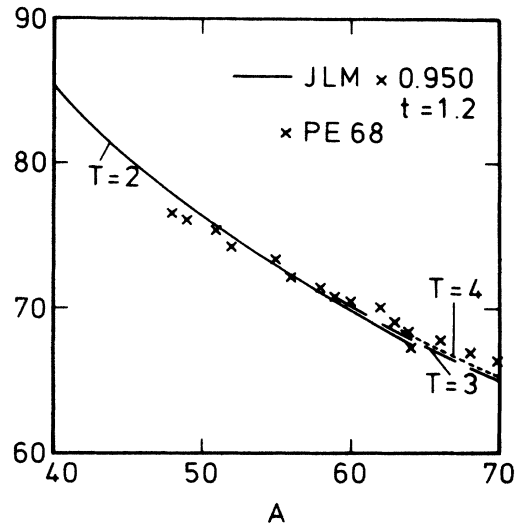

FIG. 7. Dependence upon the target mass number A of the quantity $[r^{0.4}]$ defined by Eq. (2.12). For the sake of clarity we only show (crosses) the empirical values associated with the optical potentials found in the original analysis of Perey *et al.* (Refs. 1 and 2). The curves correspond to the nuclear matter approach ($t=1.2$ fm), renormalized by a factor $\lambda_{\rm JLM}=0.95$.

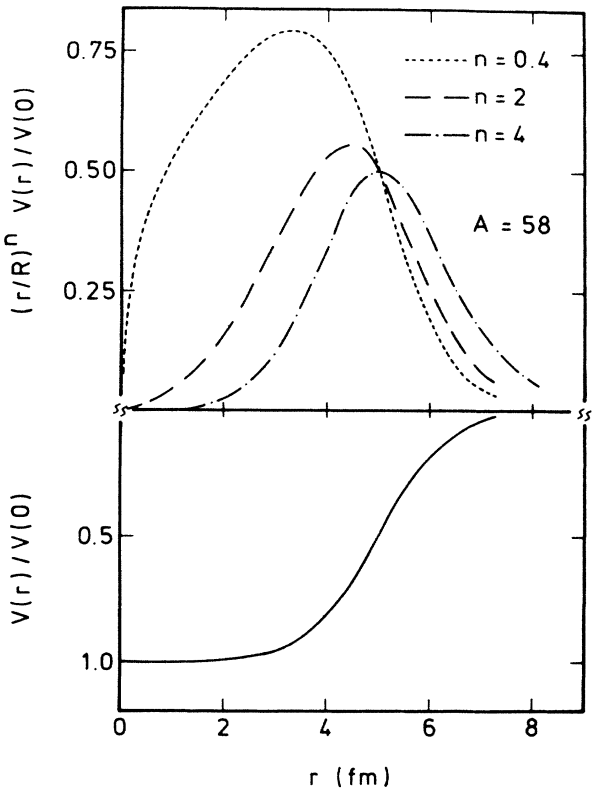

FIG. 6. Dependence upon the radial distance r of the quantities $V(r)/V(0)$ (bottom) and $(r/R)^n V(r)/V(0)$ (top) for $n=0.4$ (short-dashed line), $n=2$ (long-dashed line), and $n=4$ (dashed-dotted line), in the case of the typical optical potential defined by Eqs. (1.1)–(1.3) for $A=58$.

D. Weighting factor r^4

The radial moments

$$[r^4]=-\frac{4\pi}{A}\int V(r)r^4dr \tag{2.13}$$

are of interest because they enter in the definition of the root mean square radius. They are plotted in Fig. 8.

E. Ratios of radial moments

The quantity which is commonly used to characterize the potential range is the root mean square radius,

$$\langle r^2\rangle^{1/2}=([r^4]/[r^2])^{1/2}\,. \tag{2.14}$$

This quantity is plotted in Fig. 9.

Since the integrands which appear in the definitions of $[r^2]$ and $[r^{0.4}]$ are peaked at different locations (Fig. 6), the ratio $[r^2]/[r^{0.4}]$ also contains information on the radial shape of the potential. This ratio is plotted in Fig. 10. Its usefulness stems from the fact that $[r^{0.4}]$ is more accurately determined than $[r^4]$.

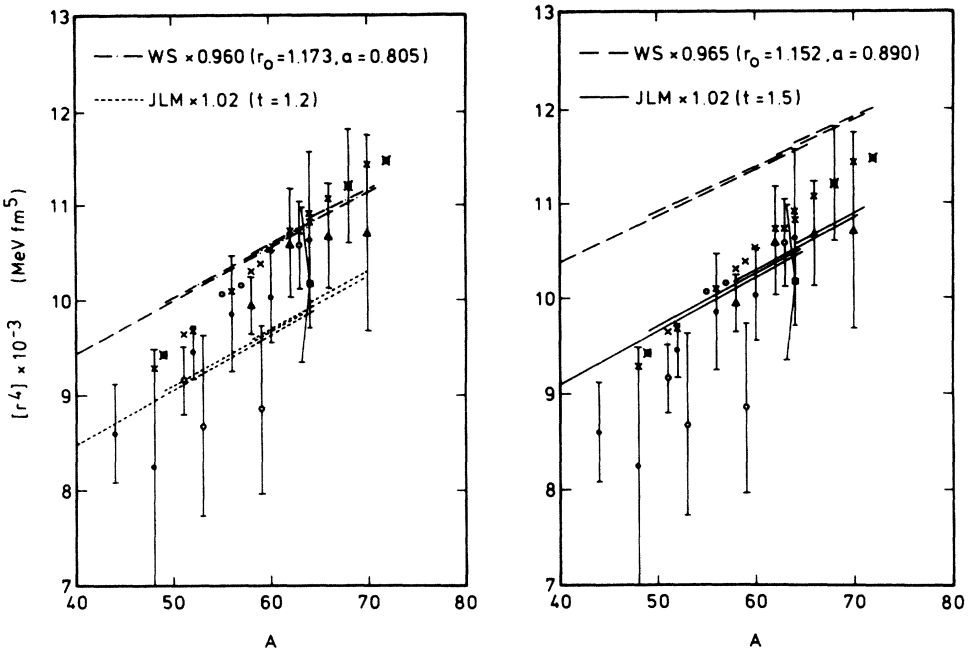

FIG. 8. Dependence upon mass number of the radial moment $[r^4]$ of the proton optical potentials. The dots, circles, triangles, and squares represent averages of the empirical values, and the vertical bars the associated standard deviations. The crosses correspond to the potentials used by Perey *et al.* (Refs. 1 and 2). In the left-hand panel, the short-dashed lines have been calculated from the nuclear matter approach of Ref. 5, with a range parameter $t=1.2$ fm; the dashed-dotted curves are associated with the corresponding Woods-Saxon fit (4.3). In the right-hand panel, the solid lines correspond to $t=1.5$ fm, while the long-dashed lines are obtained with the corresponding Woods-Saxon fit (4.4). The renormalization factors are the same as for the volume integrals (see Fig. 3).

III. COMPARISON WITH THE NUCLEAR MATTER APPROACH

A. Basic expressions

We briefly summarize the formulas of the nuclear matter approach of Ref. 5. In the "local density approximation" (LDA) the optical potential is written in the form

$$\tilde{V}(r;E)=\tilde{V}_0(r;E)+\alpha\tilde{V}_1(r;E)+\tilde{\Delta}_C(r;E)\ . \tag{3.1}$$

The isoscalar component is parametrized as follows:

$$\tilde{V}_0(r;E)=\sum_{i,j=1}^{3} a_{ij}[\rho(r)]^i E^{j-1}\ . \tag{3.2}$$

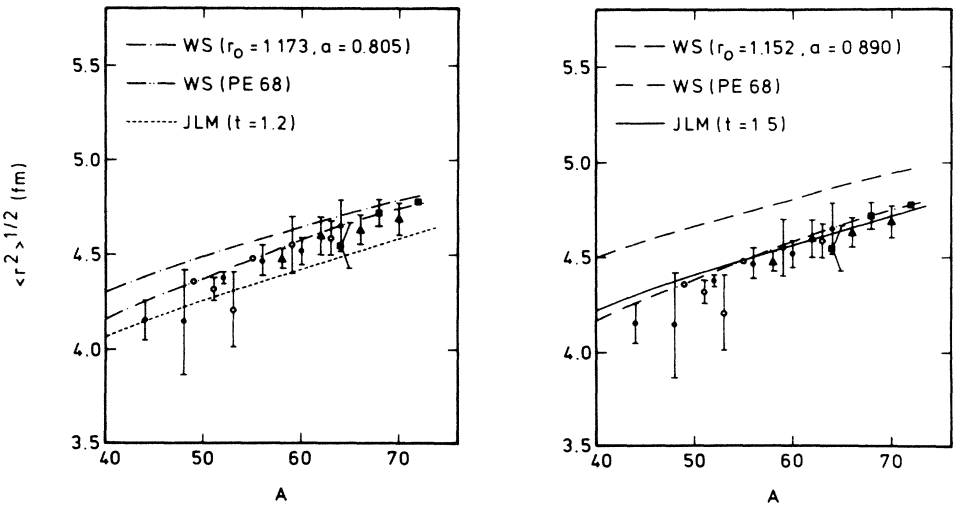

FIG. 9. Dependence of the root mean square radius upon mass number. The points represent averages of the empirical values and the vertical bars the associated standard deviations. The dashed—double-dotted curves correspond to the potentials used by Perey *et al.* (Refs. 1 and 2). The other curves represent calculated values, with the same notation as in Fig. 8; they do not involve any renormalization factor.

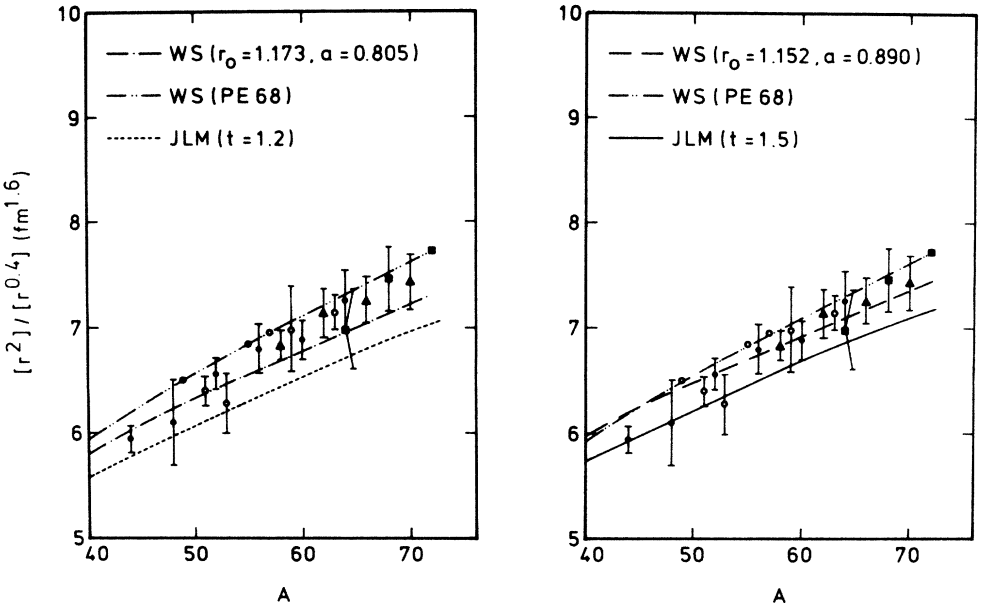

FIG. 10. Dependence upon mass number of the ratio $[r^2]/[r^{0.4}]$. The notation is the same as in Fig. 9.

The isovector component is given by

$$\tilde{V}_1(r;E)=\frac{\tilde{m}(r;E)}{m}N(r;E)\ , \tag{3.3a}$$

with

$$N(r;E)=\sum_{i,j=1}^{3} b_{ij}[\rho(r)]^i E^{j-1}\ , \tag{3.3b}$$

$$\tilde{m}(r;E)/m=1-\sum_{i,j=1}^{3} c_{ij}[\rho(r)]^i E^{j-1}\ . \tag{3.3c}$$

In Eqs. (3.2)—(3.3c), $\rho(r)$ is the matter density, which is approximated by[16]

$$\rho(r)=\rho_0\left[1+\exp\left[\frac{r-C}{b}\right]\right]^{-1}\ , \tag{3.4a}$$

where[16]

$$b=0.54\ \text{fm}\ , \tag{3.4b}$$

$$C=(0.978+0.0206A^{1/3})A^{1/3}\ \text{fm}\ , \tag{3.4c}$$

$$\rho_0=\frac{3A}{4\pi C^3}(1+\pi^2 b^2/C^2)^{-1}\ . \tag{3.4d}$$

The coefficients a_{ij}, b_{ij}, and c_{ij} are listed in Tables I—III of Ref. 5.

The Coulomb correction is given by

$$\tilde{\Delta}_C(r;E)=-\left[\frac{d}{dE}V_0(r;E)\right]V_C(r)\ , \tag{3.5a}$$

where[17,18] (r in fm, V_C in MeV)

$$V_C(r)=\begin{cases}0.719ZR_C^{-1}\left[3-\left[\dfrac{r}{R_C}\right]^2\right] & \text{for } r\le R_C\ , \quad (3.5b)\\ 1.44Z/r \quad \text{for } r>R_C\ , & (3.5c)\end{cases}$$

$$R_C=1.123A^{1/3}+2.35A^{-1/3}-2.07A^{-1}\ . \tag{3.5d}$$

In the "improved local density approximation" (ILDA) the optical potential is given by the folding formula,[5]

$$V(r;E)=(t\sqrt{\pi})^{-3}\int \tilde{V}(r';E)\times\exp[-(|\mathbf{r}-\mathbf{r}'|)^2/t^2]d^3r'\ , \tag{3.6}$$

where the Gaussian accounts for the finite range of the effective nucleon-nucleon interaction. Below, we always use the ILDA. We usually take the same value as in Ref. 5 for the range parameter t, namely

$$t=1.2\ \text{fm}\ . \tag{3.7}$$

One should not expect a very detailed agreement between the calculated quantities and the empirical ones. Indeed, the accuracy of the Bruekner-Hartree-Fock approximation in nuclear matter is about a few percent, and the ILDA introduces additional uncertainties. In particular, the ILDA is not reliable in the surface tail. In order to allow for some of these limitations, we shall multiply the calculated $V(r;E)$ by a renormalization factor λ_{JLM} which will be adjusted to improve the agreement with the empirical values (JLM denotes Jeukenne-Lejeune-Mahaux).[19–21] The deviation of λ_{JLM} from unity gives an indication of the accuracy of the nuclear matter approach of Ref. 5. Since we mainly want to investigate to what extent this approach accounts for the dependence of the empirical potentials upon A, α, and T, we shall take the same value of λ_{JLM} for all nuclei.

B. Volume integral per nucleon

In Ref. 5 it was stated that the volume integrals of V and of $\tilde{V}$ are approximately equal. In fact, these volume integrals are identical.[7] Equation (3.1) shows that one can

divide the volume integral of the proton optical potential into three components:

$$J/A = J_0/A + \alpha J_1/A + J_C/A \ . \tag{3.8}$$

With our sign convention the quantities J, J_0, J_1, and J_C are all positive.

In the case of the neutron optical potential, the volume integral per nucleon is given by

$$J_n/A = J_0/A - \alpha J_1/A \ . \tag{3.9}$$

It is found empirically that J_n/A decreases with increasing A.[10,12] Since, on the average, α increases with A [see Eq. (2.11)], the decrease of J_n/A and the fact that in the case of protons J/A is approximately independent of A entail that J_0/A should decrease with increasing A. This is in keeping with the behavior predicted by the nuclear matter approach, as exhibited in Fig. 11 for the mass numbers of interest here.

The fact that J_0/A depends upon A reflects the property that in nuclear matter the isoscalar strength V_0 is not proportional to the density ρ; see Eq. (3.2). Otherwise, one would have $\tilde{V}_0(r;E) = -\mathscr{V}_0(E)\rho(r)$ and the quantity J_0/A would be equal to

$$J_0(E)/A = \mathscr{V}_0(E) \ , \tag{3.10}$$

and would be independent of A. The dependence of J_0/A upon A is thus a consequence of the density dependence of the isoscalar component of the effective interaction. This statement holds true in the LDA as well as in the ILDA, and is independent of the radial shape adopted for the density distribution $\rho(r)$.

Srivastava *et al.*[22] have derived for J_0/A a parametric form which approximates the results of the nuclear matter approach of Ref. 5 at the energy $E=35$ MeV. This approximation reads (E in MeV)

$$J_0(E)/A = J_0'(E) f(A) \ , \tag{3.11a}$$

with

$$f(A) = 1 + 1.380A^{-1/3} + 0.516A^{-2/3} - 1.040A^{-1} \ , \tag{3.11b}$$

$$J_0'(E=35) = 270 \text{ MeV fm}^3 \ . \tag{3.11c}$$

The parametrization (3.11a) and (3.11b) has recently been used by Kwan *et al.*[9] in order to study the dependence of the volume integrals per nucleon of the neutron and proton optical potentials for nuclei with mass number $12 \le A \le 208$. These authors considered empirical data at various energies; they adopted the following expression for the coefficient $J_0'(E)$ in Eq. (3.11a):

$$J_0'(E) = 325 - 1.82E \ . \tag{3.12}$$

This yields $J_0'(E=35) = 261$ MeV fm^3, which is close to the value of Srivastava *et al.*[22]

Two remarks are in order. (i) The algebraic parametrization (3.11b) has been derived for $E=35$ MeV and is likely to become less accurate for other values of E since the calculated density dependence of V_0 depends upon energy.[5] (ii) Expression (3.11b) rests on a density distribution different from (3.4a)—(3.4d); in particular, Srivastava *et al.*[22] assumed that the density at the nuclear center is independent of A instead of being given by Eq. (3.4d).

Despite these minor remarks, the work of Kwan *et al.*[9] is of interest in the present context since it encompasses a wider range of nuclei and shows that the main features of the empirical dependence of the neutron and proton optical potentials upon the asymmetry parameter α are close to the prediction of an approximate form of the nuclear matter approach. It is therefore useful to compare the dependence upon A of the nuclear matter approach of Ref. 5 with the algebraic approximation adopted in Ref. 9. The quantity J_0/A given by Eqs. (3.11a), (3.11b), and (3.12) is represented by the short dashes in Fig. 11, for $E=11$ MeV. The dependence of J_0/A upon A is seen to be approximately the same as in the original nuclear matter approach,[5] but the normalization is approximately 5% smaller.

We recall that the quantity $\bar{\alpha}$ which appears in the abscissa of the right-hand panel of Fig. 11 only gives a rough indication of the asymmetry parameter associated with a given mass number A. For the mass numbers considered here, it is more accurate to use the exact values of $\alpha(A,T)$. The dependence of J_0/A upon the asymmetry parameter α is represented in Fig. 12, which derives from Fig. 4 and from the left-hand panel of Fig. 11. As expected from Sec. II B the smooth dependence of J_0/A upon A gives rise to a "fine structure" when J_0/A is plotted versus α.

The solid curves in Fig. 13 represent the dependence upon A and $\bar{\alpha}$ of the volume integral per nucleon of the isovector component, as calculated from the nuclear matter approach, Eqs. (3.3a)—(3.3c). The dashed lines show the parametric expression adopted by Kwan *et al.*[9]

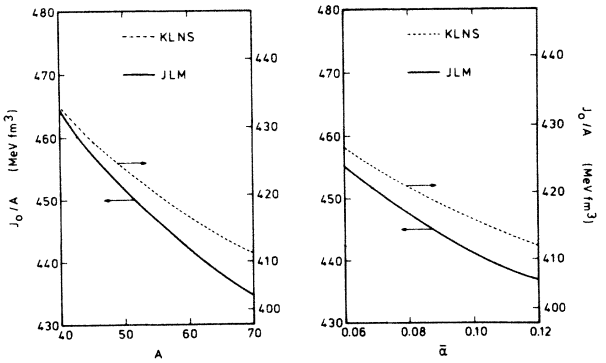

FIG. 11. The solid curve in the drawing on the left-hand side represents the dependence upon the mass number A of the volume integral per nucleon of the isoscalar component of the optical potential at 11 MeV, as calculated from the nuclear matter approach of Ref. 5 (left-hand ordinate scale). The short-dashed line represents the values (Ref. 9) given by Eq. (3.11a) with $J_0'(E=11 \text{ MeV}) = 305$ MeV fm^3 (right-hand ordinate scale). The right-hand panel represents the corresponding dependence of J_0/A upon the average asymmetry parameter $\bar{\alpha}$ defined by Eq. (2.11).

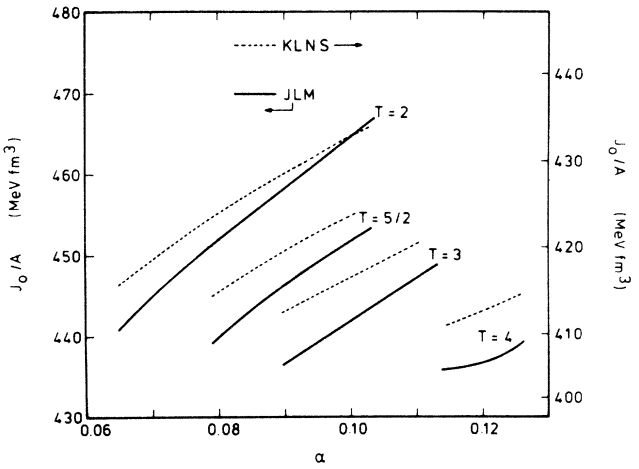

FIG. 12. Dependence upon the asymmetry parameter α of the volume integral per nucleon of the isoscalar component of the optical potential as calculated from the nuclear matter approach of Ref. 5 (solid curve, left-hand ordinate scale), and from the algebraic approximation used by Kwan *et al.* (Ref. 9) (short-dashed lines, right-hand ordinate scale).

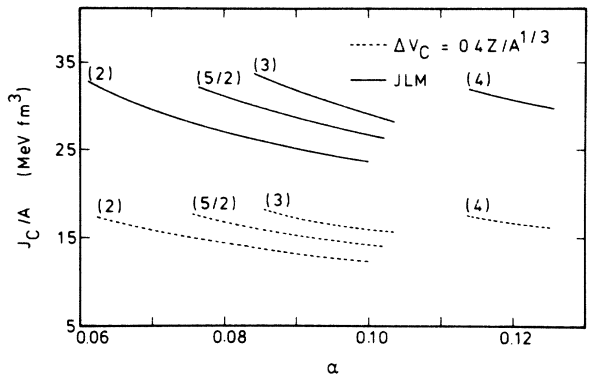

FIG. 14. Dependence upon the asymmetry parameter α of the volume integral per nucleon of the Coulomb correction. The solid lines are associated with the nuclear matter approach of Ref. 5; see Eqs. (3.5a)–(3.5d). The short-dashed lines correspond to a Woods-Saxon potential whose depth is equal to $0.4ZA^{-1/3}$ MeV, and whose geometry is fixed ($r_0=1.17$ fm, $a=0.75$ fm) (Ref. 13).

These authors assumed that the dependence of J_1/A upon A is the same as that of J_0/A,

$$J_1/A = J_1' f(A) , \tag{3.13}$$

and that $J_1'=104$ MeV fm^3 is independent of energy. This numerical value had been determined from a fit to the main features of the empirical dependence upon α of the proton optical potential for mass numbers $12 \leq A \leq 208$.

We finally turn to the volume integral per nucleon J_C/A of the Coulomb correction. The solid curves in Fig. 14 represent the values calculated from the nuclear matter approach of Ref. 5. The short dashes are associated with a standard estimate, based on a Woods-Saxon shape with a depth equal to $0.4Z/A^{1/3}$ MeV and with the "global" geometry of Becchetti *et al.*[13] The nuclear matter approach is seen to lead to values of J_C/A which are larger than those assumed in most empirical analyses.[18]

The integral per nucleon of the full optical potential is given by Eq. (3.8). Its dependence upon A as calculated from Ref. 5 is represented by the solid curves in Fig. 1, while its dependence upon α is shown by the solid curves in Fig. 3. These calculated values have been multiplied by a renormalization coefficient $\lambda_{\rm JLM}=1.02$. The agreement with the empirical values is quite satisfactory. The decrease of J_0/A with increasing A is, in part, compensated for by the increase of $\bar{\alpha}J_1/A$ with increasing A, thus resulting in a quantity J/A whose dependence upon A is weak. This dependence is, however, slightly more pronounced than that of the empirical values. This is due to the fact that the calculated dependence of J_0/A upon A is somewhat too strong, presumably reflecting an overly strong density dependence of the effective interaction.

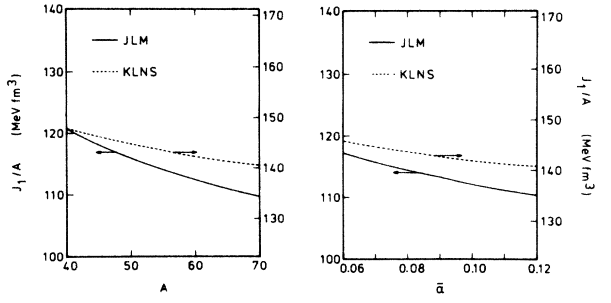

FIG. 13. Same as Fig. 11, for the volume integral per nucleon of the isovector component of the optical potential.

The values of J/A can also be calculated from the semimicroscopic values adopted by Kwan *et al.*[9] We assumed that these authors used the Coulomb correction J_C/A represented by the short dashes in Fig. 14. If the results of Kwan *et al.*[9] are renormalized by a factor $\lambda_{\rm KLNS}=1.095$ (KLNS denotes Kwan-Lam-Neilson-Sherif), the resulting values of J/A for $E=11$ MeV and $T=2$ practically coincide with the solid curve in Fig. 1. However, the values of J/A for $T=4$ are larger in the case of Ref. 9 (short dashes in Fig. 1) than in the case of Ref. 5 (solid curve in Fig. 1). This reflects the fact that the values of J_1/A adopted in Ref. 9 are larger than those calculated in Ref. 5.

C. Weighting factors $r^{0.4}$, r^4, and ratios of radial moments

The theoretical values of the quantity $[r^{0.4}]$ defined by Eq. (2.12) can be calculated from the nuclear matter approach of Ref. 5. In contrast to the volume integral per nucleon, they depend upon the choice of the range parameter t which appears in Eq. (3.6).

We first consider the results associated with the value $t=1.2$ fm originally adopted in Ref. 5. The correspond-

ing quantity $[r^{0.4}]$ is represented by the short dashes in Fig. 5, after renormalization by a factor $\lambda_{JLM}=0.95$. A 5% change in the normalization appears to be in keeping with the overall accuracy expected for the nuclear matter approach. However, it is not satisfactory that the renormalization coefficient ($\lambda_{JLM}=0.95$) which must be introduced in the case of $[r^{0.4}]$ differs from that ($\lambda_{JLM}=1.02$) which had been adopted in the case of J/A. This difference is reflected by the fact that in the case $t=1.2$ fm the calculated values of the ratio $[r^2]/[r^{0.4}]$ are too small; see Fig. 10. This indicates that the radial shape of the calculated potential is not in detailed agreement with the empirical shapes.

Another way of exhibiting this defect of the theoretical calculation consists of comparing the empirical root mean square radii with those calculated from the nuclear matter approach. This is performed in Fig. 9, which shows that in the case $t=1.2$ fm the nuclear matter approach yields overly small root mean square radii. One could try to improve the agreement by changing the value of the range parameter t. The solid curve in Fig. 9 shows that the value of $t=1.5$ fm leads to a good agreement between the calculated and empirical values of the root mean square radii. However, the solid curve in Fig. 10 shows that the corresponding ratio $[r^2]/[r^{0.4}]$ remains too small. This is reflected in Fig. 5, where the solid curves correspond to $t=1.5$ fm with a renormalization factor $\lambda_{JLM}=0.975$. The latter value is still smaller than that (1.02) needed in the case of the volume integral.

IV. POTENTIAL SHAPE

The short dashes and solid curve in Fig. 15 show the shape of the optical potential of ^{66}Zn, as calculated from the nuclear matter approach for the range parameters $t=1.2$ and 1.5 fm, respectively. We saw in the preceding section that these calculated shapes are not in very good agreement with the empirical evidence, since there exists a difference between the renormalization factors λ_{JLM} which had to be introduced for J/A ($\lambda_{JLM}=1.02$) on one hand, and for $[r^{0.4}]$ ($\lambda_{JLM}=0.95$ for $t=1.2$ fm, $\lambda_{JLM}=0.975$ for $t=1.5$ fm) on the other.

One plausible explanation for this difference lies in the fact that the ILDA is not reliable in the surface tail, while this region influences the value of J/A. It is therefore of interest to construct a Woods-Saxon potential which closely fits the calculated potential, except in the surface tail. We proceed as follows. We request the parameters U, r_0, and a in Eq. (1.1) to have the following properties:

$$U=2V(R)\,, \tag{4.1}$$

$$a=(r_{0.1}-r_{0.9})/4.39\,; \tag{4.2}$$

here, $V(r)$ is the calculated potential, while r_q is defined by $V(r_q)=qU$. Since U is slightly different from $V(r=0)$, the parameters r_0 and a must be determined by iteration. We obtained the following values,

$$r_0=1.173 \text{ fm},\quad a=0.805 \text{ fm}\,, \tag{4.3}$$

in the case of the potential calculated with the range parameter $t=1.2$ fm, and

$$r_0=1.152 \text{ fm},\quad a=0.890 \text{ fm} \tag{4.4}$$

in the case $t=1.5$ fm. These parameters are practically the same for all the nuclei considered here. In contrast, the depth U of the Woods-Saxon fit is not the same for all nuclei. This is illustrated by the dashed-dotted curve in

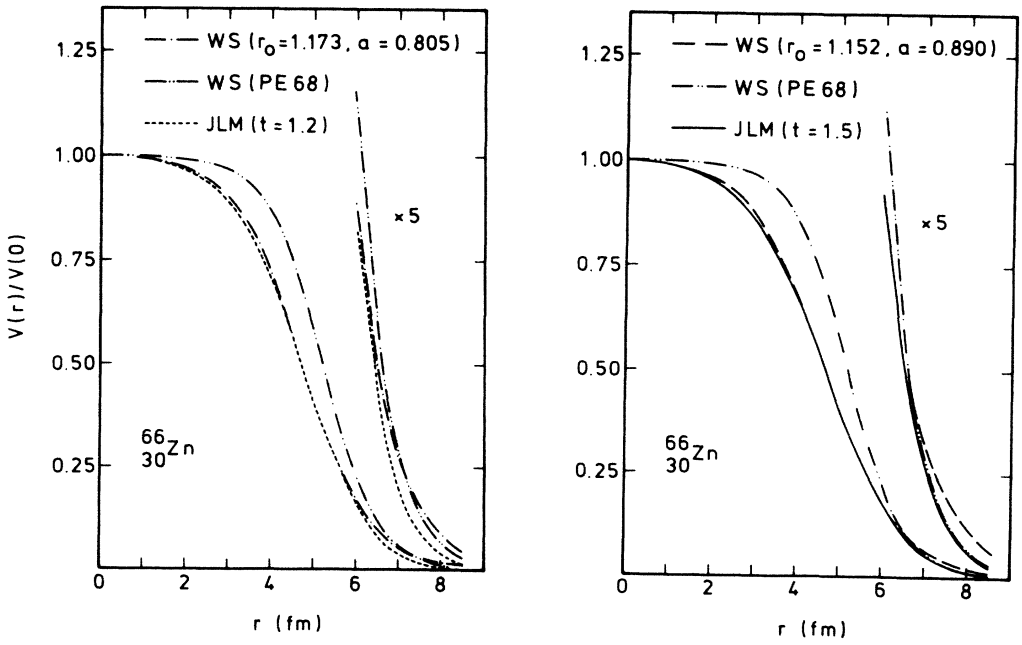

FIG. 15. Radial shape of $V(r)/V(0)$ in the example of ^{66}Zn. The notation is the same as in Fig. 9.

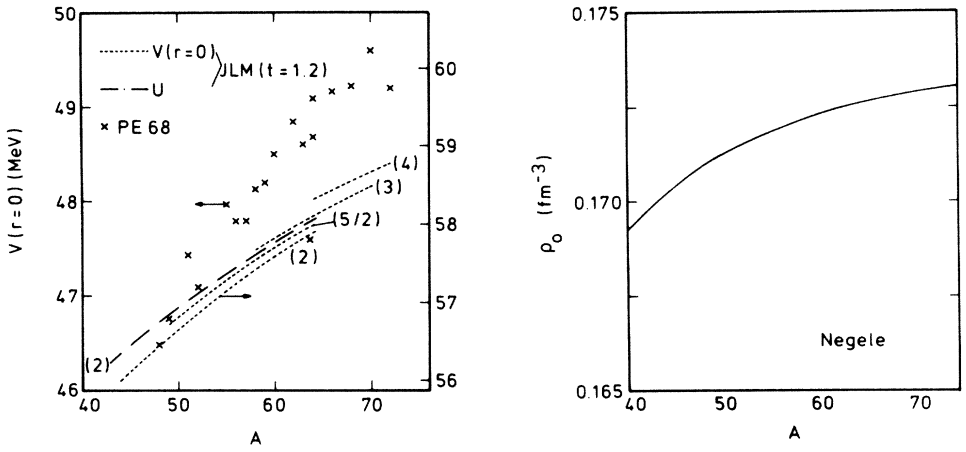

FIG. 16. The left-hand panel shows the dependence of the proton optical potential depth upon mass number. The crosses correspond to the empirical values of Perey *et al.* (Refs. 1 and 2). The short-dashed lines (right-hand scale) represent the values of $V(r=0)$ as calculated from the nuclear matter approach ($t=1.2$ fm). Their increase with A partly reflects that of ρ_0, which is represented by the solid curve on the right-hand side. The dashed-dotted line represents the value of $U=V(r=0)[1+\exp(-R/a)]$, in the case $T=2$, where $R=r_0A^{1/3}$ and a are taken from Eq. (4.3).

Fig. 16. The increase of U with A essentially reflects the increase of ρ_0 with A [see Eq. (3.4d) and the right-hand panel of Fig. 16].

Figure 15 shows that the Woods-Saxon shape closely fits that of the calculated potentials, except in the surface tail, where the nuclear matter approach is unreliable and where the extrapolation of a Woods-Saxon shape is physically quite reasonable. From the values of r_0, a, and U one can calculate the quantities $[r^2]=J/A$, $[r^{0.4}]$, $[r^4]$, $\langle r^2\rangle^{1/2}$, and $[r^2]/[r^{0.4}]$. The results are represented in Figs. 3, 5, 8, 9, and 10. The renormalization factors requested to fit the empirical values of $[r^2]$ and $[r^{0.4}]$ only differ by about 2% in the case of the Woods-Saxon fit to the nuclear matter results associated with $t=1.2$ fm. Moreover, it is remarkable that the empirical values of $[r^4]$, and correspondingly of $\langle r^2\rangle$, are also closely reproduced by this Woods-Saxon fit.

We can thus conclude that the nuclear matter approach of Ref. 5 ($t=1.2$ fm) is in quite good agreement with the empirical optical potentials, provided one adopts a physically reasonable extrapolation in the surface tail. Three remarks are in order. (i) No parameter was adjusted except for an overall renormalization factor $\lambda_{\rm JLM}=0.95\pm0.01$. The deviation of this factor from unity is in keeping with the fact that in nuclear matter the Bruekner-Hartree-Fock approximation overestimates the magnitude of the potential energy by a few percent.[23] (ii) The geometrical parameters (4.3) and (4.4) of the Woods-Saxon fits to the calculated potentials are quite different from those, (1.3), adopted by Perey *et al.*[2] in their original analysis. (iii) The range parameter $t=1.2$ fm is the same as that adopted in the original theoretical model.[5] The Woods-Saxon fit associated with the larger value $t=1.5$ fm yields overly large root mean square radii, as shown by the long dashes in the right-hand panel of Fig. 9.

V. DISCUSSION

The analyses of elastic scattering data do not enable one to accurately determine the detailed shape of the optical potential, but only its global properties. The latter can be characterized by the volume integral per nucleon, $[r^2]=J/A$ [Eq. (2.1)], and by the moments $[r^{0.4}]$ and $[r^4]$, Eqs. (2.12) and (2.13). The moment $[r^4]$ is usually combined with $[r^2]$ to yield the mean square radius $\langle r^2\rangle$, which is one of the characteristics of the potential shape, another characteristic being the ratio $[r^2]/[r^{0.4}]$. We have performed extended compilations of the empirical values of $[r^2]$, $[r^{0.4}]$, $[r^4]$, $\langle r^2\rangle^{1/2}$, and $[r^2]/[r^{0.4}]$. These quantities are found to be smooth functions of the target mass number A in the case of 11 MeV protons and of targets with mass number $44\leq A\leq 72$. This is exhibited by Figs. 1 and 7–10.

If the potential is assumed to have a Woods-Saxon shape [Eq. (1.1)], its volume integral is given by

$$J=\frac{4\pi}{3}UR^3\left[1+\pi^2\frac{a^2}{R^2}\right]. \tag{5.1}$$

In their original analysis, Perey *et al.*[1,2] assumed that the potential has a Woods-Saxon shape, with a and $r_0=RA^{-1/3}$ independent of A. Then, the observation that J/A is approximately independent of A (Fig. 1) combined with Eq. (5.1) implies that the potential depth U increases with increasing values of A (Fig. 16). This entails that the empirical values of the depth U presents a fine structure, i.e., fall on a set of distinct curves when plotted versus α, each curve being labeled by the isospin T. Indeed, the relation $A=2T/\alpha$ implies that a quantity which is a smooth function of A is represented by a family of curves when plotted versus α, each curve being

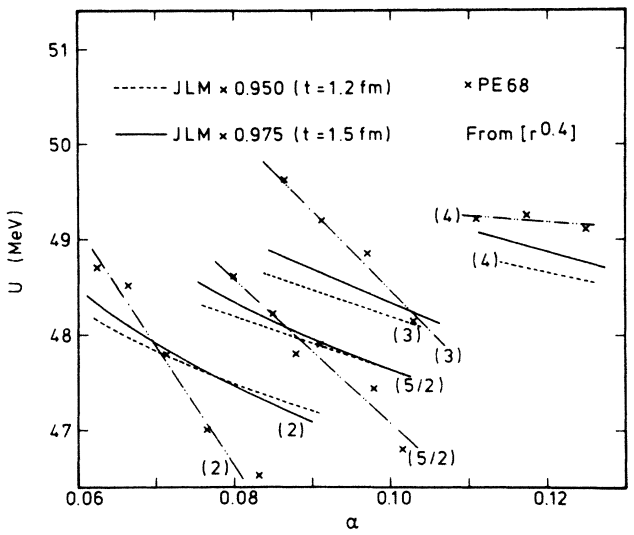

FIG. 17. Dependence upon the asymmetry parameter of optical potential depths which yield specific values of $[r^{0.4}]$ and are associated with a Woods-Saxon shape with the fixed geometry specified by Eq. (1.3). The crosses are associated with the empirical values given by Perey *et al.* (Ref. 2). The dashed–double-dotted lines have been drawn by eye through these empirical values. The solid curves and the short-dashed lines correspond to the calculated values of $[r^{0.4}]$ represented by the solid curves and the short-dashed lines shown in Fig. 5.

characterized by a given value of T. This "fine structure" is exhibited in Fig. 17.

One should not expect a very detailed agreement between the empirical fine structure and the results of the nuclear matter approach. Indeed, the latter involves several approximations which limit its accuracy to a few percent, which is the magnitude of the empirical fine structure. Among these approximations, we recall the local density approximation, the assumed shape of the matter density distribution, the possible existence of a neutron-rich surface skin, and the existence of polarization corrections. The latter may affect the shape of the potential, particularly at the nuclear surface.[24] However, the polarization corrections are unlikely to be mainly responsible for the fine structure. Indeed, it has recently been observed[25] that the fine structure also appears when the Fermi energy is plotted versus α, while the polarization corrections are negligible at the Fermi energy.[24] The present study shows that the main origin of the fine structure lies in the A dependence of the isoscalar contribution, which, in turn, reflects the density dependence of the effective nucleon-nucleon interaction. The fine structure is therefore expected to emerge from a Hartree-Fock calculation based on a density-dependent effective interaction, but not from one based on a density-independent interaction.

The fine structure appears *within* the stability band. When a wide range of mass numbers is considered, the *average* value $\bar{\alpha}$ of the asymmetry parameter increases with A; see Eq. (2.11). In the case of protons, the volume integral per nucleon, J/A, is approximately independent of A and of the average asymmetry parameter $\bar{\alpha}$ because the increase with A of the isovector contribution $\bar{\alpha}J_1/A$ is almost compensated for by the decrease of the isoscalar contribution J_0/A.

The local density approximation is unreliable in the surface tail. Therefore it appears preferable not to use the calculated potential in this domain. This is why we have constructed a Woods-Saxon potential which closely reproduces the calculated shape except in the tail. This potential turns out to have a fixed geometry [Eq. (4.3)] in the mass region $44 \leq A \leq 72$ studied here. It leads to a very good agreement with the radial moments of the empirical potentials, provided that a renormalization factor ($\lambda_{\rm JLM}=0.95\pm0.01$) is introduced. The fact that this factor is slightly smaller than unity agrees with the expectation that the Bruekner-Hartree-Fock approximation overestimates the strength of the optical potential in nuclear matter.

We suggest that in future comparisons between experimental data and the nuclear matter approach (see, e.g., Refs. 19–21), the latter should be modified to take into account its inaccuracy in the surface tail, for instance, by using the procedure described in Sec. IV.

The surface tail significantly influences the calculated values of the volume integral J and of the mean square radius $\langle r^2 \rangle$. Caution must therefore be exercised if one wants to derive theoretical information on the geometrical properties of the optical potential from calculated values of $\langle r^2 \rangle$.[3,26,27]

[1]C. M. Perey and F. G. Perey, Phys. Lett. **26B**, 123 (1968).
[2]C. M. Perey, F. G. Perey, J. K. Dickens, and R. J. Silva, Phys. Rev. **175**, 1460 (1968).
[3]P. E. Hodgson, in *Neutron-Nucleus Collisions. A Probe of Nuclear Structure,* edited by J. Rapaport, R. W. Finlay, S. M. Grimes, and F. S. Dietrich, AIP Conf. Proc. No. 124 (American Institute of Physics, New York, 1985), p. 1.
[4]P. E. Hodgson, Nucl. Phys. **A150**, 1 (1970).
[5]J.-P. Jeukenne, A. Lejeune, and C. Mahaux, Phys. Rev. C **16**, 80 (1977).
[6]C. M. Perey and F. G. Perey, At. Data Nucl. Data Tables **17**, 1 (1976).
[7]G. W. Greenlees, G. J. Pyle, and Y. C. Tang, Phys. Rev. **171**, 1115 (1968).
[8]F. G. Perey, in *Nuclear Spectroscopy and Reactions,* edited by J. Cerny (Academic, New York, 1974), Pt. B, p. 137.
[9]S. P. Kwan, S. T. Lam, G. C. Neilson, and H. S. Sherif, Phys. Rev. C **31**, 271 (1985).
[10]S. Kailas and S. K. Gupta, Phys. Rev. C **17**, 2236 (1978).
[11]S. Kailas, M. K. Mehta, S. K. Gupta, Y. P. Viyogi, and N. K. Ganguly, Phys. Rev. C **20**, 1272 (1979).
[12]J. Rapaport, Phys. Rep. **87**, 25 (1982).
[13]F. D. Becchetti and G. W. Greenlees, Phys. Rev. **182**, 1190 (1969).
[14]C. Mahaux and R. Sartor, Nucl. Phys., in press.
[15]C. Mahaux and R. Sartor, in *Proceedings of the Specialists'*

Meeting on the Use of the Optical Model for the Calculation of Neutron Cross Sections below 20 MeV (OECD, Paris, 1986), p. 17.

[16]J. W. Negele, Phys. Rev. C **1**, 1260 (1970).

[17]L. R. B. Elton, *Nuclear Sizes* (Oxford University Press, London, 1961), p. 36.

[18]J.-P. Jeukenne, A. Lejeune, and C. Mahaux, Phys. Rev. C **15**, 10 (1977).

[19]S. Mellema, R. W. Finlay, F. S. Dietrich, and F. Petrovich, Phys. Rev. C **28**, 2267 (1983).

[20]L. F. Hansen, F. S. Dietrich, B. A. Pohl, C. H. Poppe, and C. Wong, Phys. Rev. C **31**, 111 (1985).

[21]J. S. Petler, M. S. Islam, R. W. Finlay, and F. S. Dietrich, Phys. Rev. C **32**, 673 (1985).

[22]D. K. Srivastava, N. K. Ganguly, and D. N. Basu, Phys. Lett. **125B**, 260 (1983).

[23]C. Mahaux, in *Microscopic Optical Potentials,* edited by H. V. von Geramb (Springer-Verlag, Berlin, 1979), p. 1.

[24]C. Mahaux and H. Ngô, Nucl. Phys. **A378**, 205 (1982).

[25]Y. Wang and J. Rapaport, Nucl. Phys. **A454**, 359 (1986).

[26]D. K. Srivastava, Phys. Lett. **113B**, 353 (1982).

[27]D. K. Srivastava, D. N. Basu, and N. K. Ganguly, Phys. Lett. **124B**, 6 (1983).